Supporting Information – Impact of SWCNT Processing on Nanotube-Silicon Heterojunctions

John M. Harris,[§] *Robert J. Headrick,*[¶+] *Matthew R. Semler,*[§] *Jeffrey A. Fagan,*[†] *Matteo Pasquali,*[¶+#] *and Erik K. Hobbie**[§‡]

[§] Department of Physics, North Dakota State University, Fargo, North Dakota 58108

[¶] Department of Chemistry, Rice University, Houston, Texas 77005

[+] Richard E. Smalley Institute for Nanoscale Science and Technology, Rice University, Houston, Texas 77005

[†] National Institute of Standards and Technology, Gaithersburg, Maryland 20899

[#] Department of Chemical and Biomolecular Engineering, Rice University, Houston, Texas 77005

[‡] Department of Coatings & Polymeric Materials, North Dakota State University, Fargo, North Dakota 58108

SWCNT Purification

Enrichment in (6,5) chirality was achieved using the aqueous two-phase extraction (ATPE) approach.[1,2] CoMoCat (Southwest nanotechnologies lot SG65EX or SG65i lot 046) SWCNTs - the same nanotubes used for the unsorted films - were obtained from the manufacturer and utilized without modification. Sodium deoxycholate (Bioxtra, 98+ %), sodium dodecyl sulfate (> 99 %), and sodium cholate (SC, > 99 %) were purchased from Sigma-Aldrich and used without additional purification. NaClO (10-15 % solution) was obtained from Sigma-Aldrich and diluted 1:99 with H_2O to generate stock solutions. Polyethylene glycol (PEG, 6 kD) was purchased from Alfa Aesar and dextran 70 was

obtained from TCI (lot # BMGYL-TK). Stock solutions of PEG and Dextran were prepared by mass/mass ratio and stock surfactant solutions were prepared by mass/volume ratio. All subsequent solutions obtained from these stock solutions were made by volumetric dilution.

Iterative diameter separation by ATPE[2] was performed *via* the addition of known volumes of top- or bottom-phase mimics to the SWCNT-rich opposite phase. These mimics were comprised of 16 % dextran, 0 % PEG, 0.05 % DOC, 0 % SDS for the bottom, and 0 % (mass/mass) dextran, 12.5 % PEG, 0.4 g/L DOC and X % SDS for the top, where X was varied depending on the desired SDS concentration difference (most often 0.4 %, 0.6 %, or 1.2 %). The final fractions were concentrated and pushed to the top (PEG-rich) phase to ease processing and optical measurements. An equal volume of 20 g/L DOC was added to each separated fraction to ensure stability and enable spectroscopy. To obtain AFM images, 20 μL of solution was diluted with 100 μL of DI water to reduce the SWCNT and surfactant concentration. A small chip of silicon wafer was UVO-plasma cleaned and then placed in the solution for 24 hours in a refrigerator, after which it was removed and dried in air. The chips were then soaked in ethanol for 4 h to remove surfactant, dried in air, and imaged with AFM. Length/diameter distributions were measured with ImageJ in a manner that ignores bundles.

Film Preparation

To process the (6,5)-enriched surfactant-laden nanotubes, a 250 mL solution of 10 % ethanol in DI water was prepared in a vacuum filtration apparatus over mixed cellulose ester (MCE) filter paper to prepare surfactant-free films. An aqueous solution of surfactant-stabilized (6,5)-enriched SWCNTs was then slowly pipetted onto the MCE

surface. To ensure film uniformity, the SWCNT-rich interlayer was allowed to settle before applying vacuum. Excess surfactant was removed by repeated rinsing of the MCE-supported films. After filtration, the MCE was thoroughly rinsed in DI water and vacuum dried. The films ranged in thickness from (20 to 120) nm as measured with AFM on silicon wafer substrates. The films were collected as free-floating sheets in ethanol (Fig. 1d, main text), which served as feedstock for processing in chlorosulfonic acid (CSA).

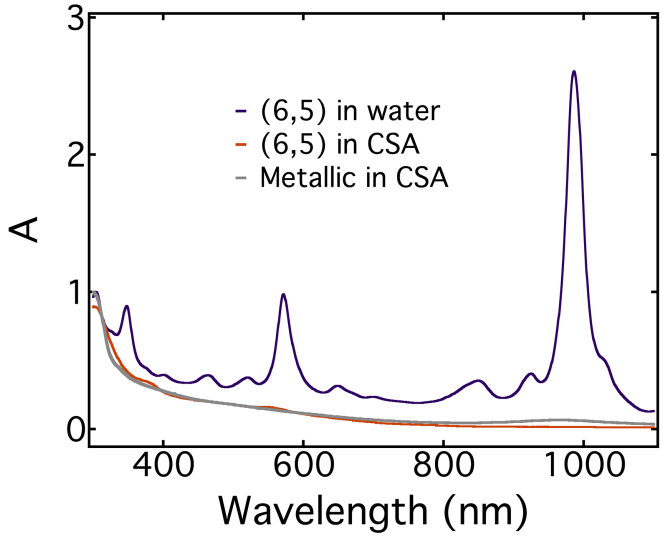

Figure S1 - Impact of CSA doping on the absorption spectrum of (6,5)-enriched SWCNT suspensions. A metallic-enriched suspension in CSA is shown for comparison.

For the unsorted films, SG65i and SG65EX CoMoCat SWCNTs were provided by SouthWest NanoTechnologies. Chlorosulfonic acid and diethyl ether were purchased from Sigma Aldrich. Thin films were produced by solution processing in CSA, which acts as a true solvent and strong dopant for CNTs (Fig. S1).[4,5] Isotropic films were fabricated by filtration through an alumina membrane.[6] SWCNTs were dissolved in CSA at 600 ppm by stir-bar mixing and diluted to 1 to 5 ppm depending on the desired film thickness. Dilute SWCNT solutions were vacuum filtered through an Anodisc alumina

membrane with an average pore size of 20 nm and finally rinsed with chloroform to remove residual acid. Aligned films (Fig. S2) were fabricated by a slide-coating method.[7] Briefly, SWCNTs were dissolved into CSA at 600 to 2,500 ppm by stir-bar mixing and a small volume of the solution was pipetted between two glass slides. The pieces of glass were slid in opposite directions, shearing the fluid and aligning the SWCNTs. To coagulate the films, the coated glass slides were dipped into diethyl ether, causing the SWCNTs to solidify onto the glass substrates. After acid removal, the isotropic and aligned SWCNT films were floated onto a water bath for transfer.

To prepare devices, the CSA-processed films were deposited on patterned Si substrates using two different approaches. In the first, the films were floated off glass onto DI water and recovered on MCE filter paper. After drying, the filter paper was cut into 3 mm squares, which were dropped into a 20 mL acetone bath prior to use. The MCE quickly dissolves to yield free-floating SWCNT films. After 1 h of gentle rinsing, films were collected in a pipette tip with acetone, where proper pipette pressure allowed retention of the film while the acetone was drained. Fresh acetone was then collected to deposit a film into a clean vial of acetone for an additional hour. This process was repeated across three 20 mL acetone baths and subsequently across three 20 mL ethanol baths. After the third and final ethanol bath, the film was collected in a clean pipette tip with ethanol and deposited on the device. Droplets of ethanol were used to orient and unfurl the film and air from a pipette was used to position the film on the patterned substrate while the ethanol evaporated.[3] In the second approach, CSA-processed SWCNT films were floated off glass substrates onto the surface of a DI water bath. These films were then collected from the water surface directly onto patterned device substrates.

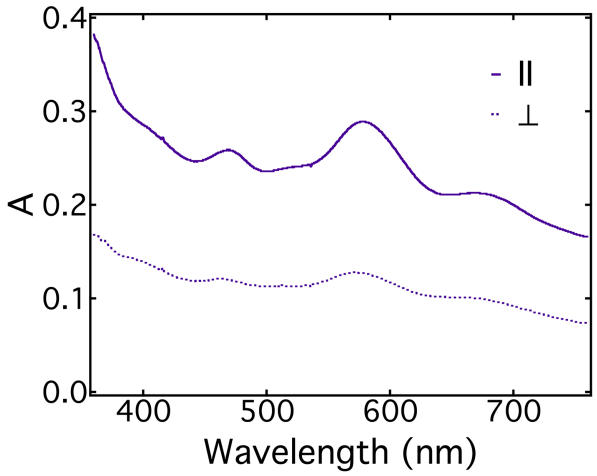

Figure S2 - Absorption spectra of a dry aligned unsorted film near the S_{22} transition for light polarized along (parallel) and normal (perpendicular) to the axis of alignment.

Device Fabrication

Wafers of n-type ⟨100⟩ crystalline silicon (n-Si, 0.4 Ω cm) were submerged in an H_2O_2/H_2SO_4 mixture, buffered oxide etch (BOE), and H_2O_2/HCl (80 °C) in intervals of 10, 1, and 10 min, respectively. A 600 nm silicon dioxide (SiO_2) layer was then grown on the wafer and patterned into a grid using photolithography in conjunction with BOE. Excess photoresist was removed using acetone. The bottom of the wafer was coated with 250 nm of Aluminum (Al) *via* magnetron sputtering and annealed at 250 °C for 2 hours to create a bottom contact with a minimal metal-Si Schottky barrier. Using bi-layer photolithography, the top surface was coated with both polymethylglutarimide (PMGI) and a standard positive photoresist before being exposed and developed to clear regions aligned over the SiO_2 dielectric but narrower along each edge by 10-15 μm. The top surface was covered with Cr/Au/Cr (maintained under vacuum) at thicknesses of 10, 100, and 10 nm, respectively. The wafer was then soaked overnight in N-methyl-2-pyrrolidone (NMP) to dissolve photoresist and remove excess metal.

Doping, Device Active Area, and Masking

All films had residual doping effects associated with CSA processing. On top of this, the 3-part chemical doping process consisted of (1) washing the active area with 1 % HF to remove oxides, (2) chemical doping with a few drops of thionyl chloride ($SOCl_2$), and (3) chemical doping *via* spin coating 1.32 mg/g of gold chloride ($AuCl_3$) in nitromethane (CH_3NO_2). The typical evolution of the *I-V* characteristics for three devices during the 3-step doping sequence is shown in Fig. S3.

The devices were masked both digitally, using a large database of high-quality devices having varied active area, and physically, using an opaque mask designed to reveal only the nine fundamental squares of the grid (active area = 0.09 cm^2). For digitally masked devices, the initial active area of a device is the total area of SWCNT in apparent contact with the underlying wafer. It was measured with an optical microscope and was always of order 0.1 cm^2. Such data were then corrected for the geometrical effects shown in Fig S4 by extrapolating to the targeted active area of 0.09 cm^2. The absence of a contribution to the photocurrent from illuminated areas of bare silicon outside of the grid was confirmed by physically masking devices. In terms of device performance, similar results were obtained for both digital masking and physical masking (Fig. S5), with a maximum short-circuit current density near 25 mA/cm^2.

Device Characterization and Sheet Resistance

Light (AM1.5) and dark *I-V* profiles were measured using an SS50AAA solar simulator (Photo Emission Tech) in conjunction with a Keithley 2400 source meter. The reverse recovery time was measured using a BK Precision 4011A function generator with a square wave potential offset at -2 V to 5 V at a frequency of 3.55 kHz in series with a

200 Ω resistor. A Tektronix TDS3034B oscilloscope was used to record the transient response to the asymmetric bias jump. Select devices were placed on a temperature-controlled plate inside an Agilent B1500A semiconductor analyzer and the dark *I-V* curves were measured at 20 degree intervals from 20 °C to 120 °C.

Two approaches were employed to measure sheet resistance. First, a rectangular SWCNT film was deposited on a quartz substrate and two interdigitated Au/Cr electrodes were sputtered onto the film without breaking vacuum. A frequency dependent measurement (1 kHz to 1 MHz, Agilent B1500A) was then used to extract the complex impedance of the film, which was converted to sheet resistance using the measured geometry and dimensions of the film. This method was complemented using a static 4-point probe measurement, where both approaches yielded comparable results.

Film Transparency and Absorption Spectroscopy

The SWCNT films of varied thickness as determined by AFM were deposited on quartz substrates and placed in the beam-path of a Cary 5000 UV-Vis-NIR spectrometer. The substrate spectrum was subtracted from the signal to yield the absorption spectrum of the SWCNTs over the wavelength interval 200-2000 nm.

SWCNT films of varied AFM thickness deposited on quartz were also measured in a transmission optical microscope equipped with an Ocean Optics USB2000 spectrometer and a broad-wavelength white light source. The ratio of the transmitted spectral intensity to that transmitted through the bare substrate was used to obtain the transmittance of the SWCNT films over a window of 400-750 nm.

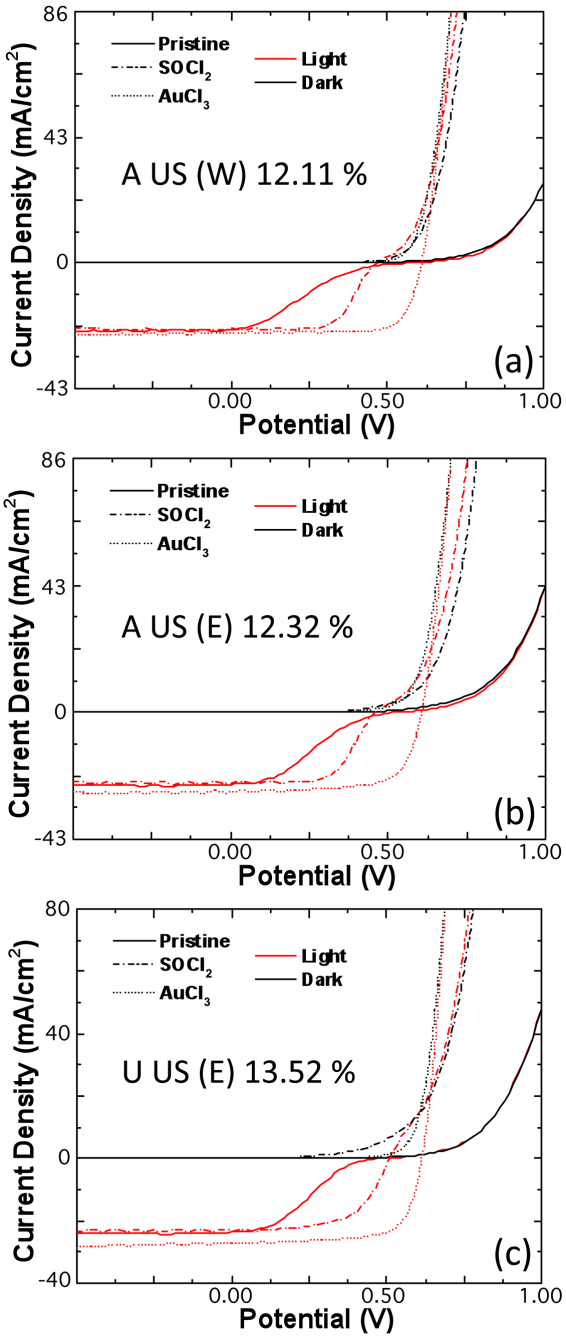

Figure S3 - Sequential I-V curves through the doping cycle for some of the top performing devices detailed in the main text.

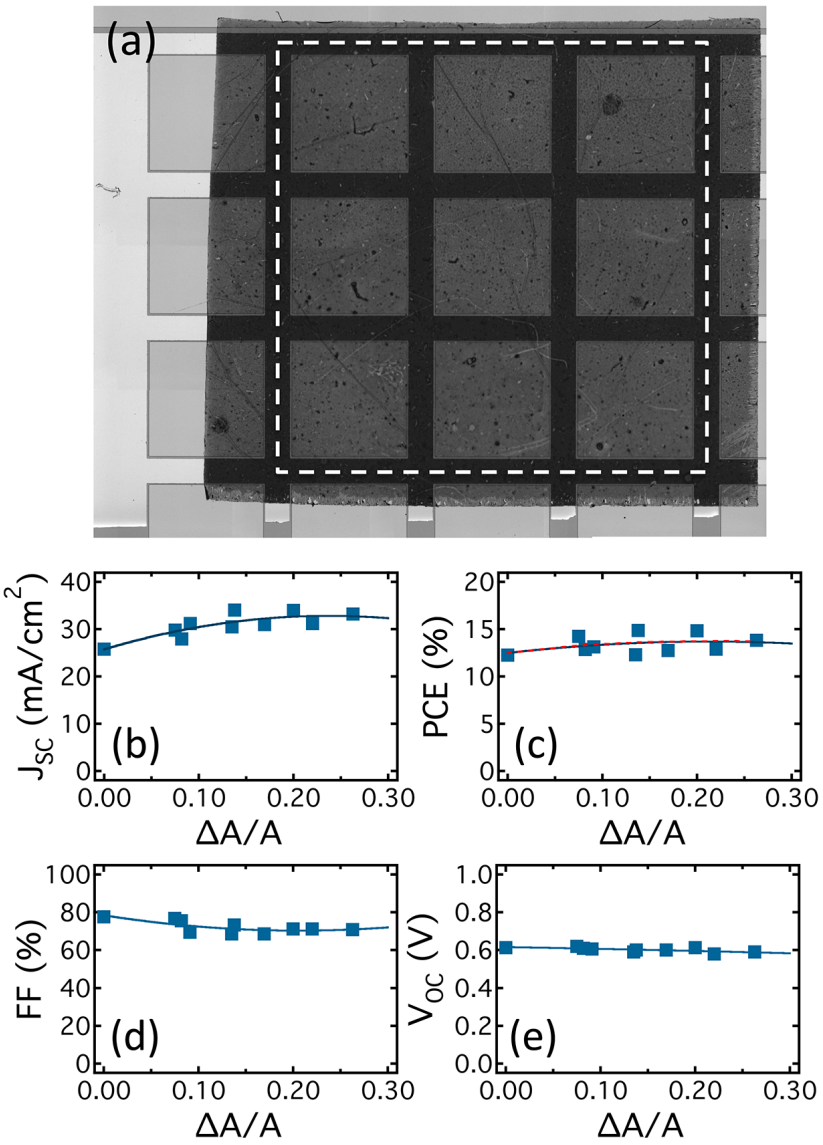

Figure S4 - (a) A device consisting of a SWCNT film (dark) on top of a silicon wafer (gray) patterned with an insulated electrode (light). (b)-(e) Characteristics of some of the top performing devices as a function of $\Delta A/A$, highlighting the digital masking approach. Devices that were physically masked by covering all area outside of the dashed square with an opaque (black) mask gave similar results, with a maximum short-circuit current density of around 25 mA/cm^2 for the highest quality devices.

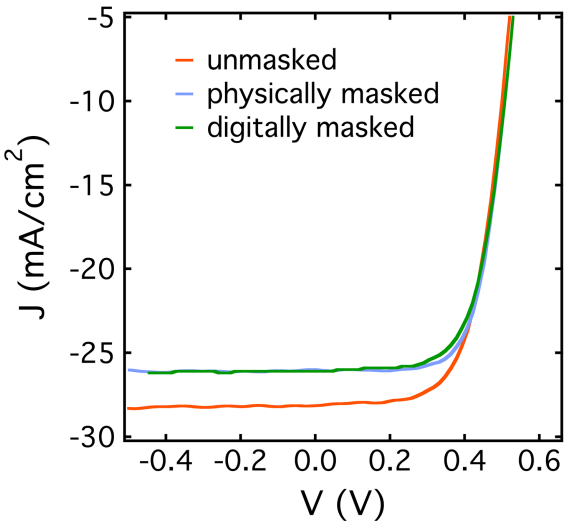

Figure S5 - A comparison of the unmasked (red), physically masked (blue) and digitally masked (green) photo-response for a better performing device with $\Delta A/A$ = 0.05-0.075.

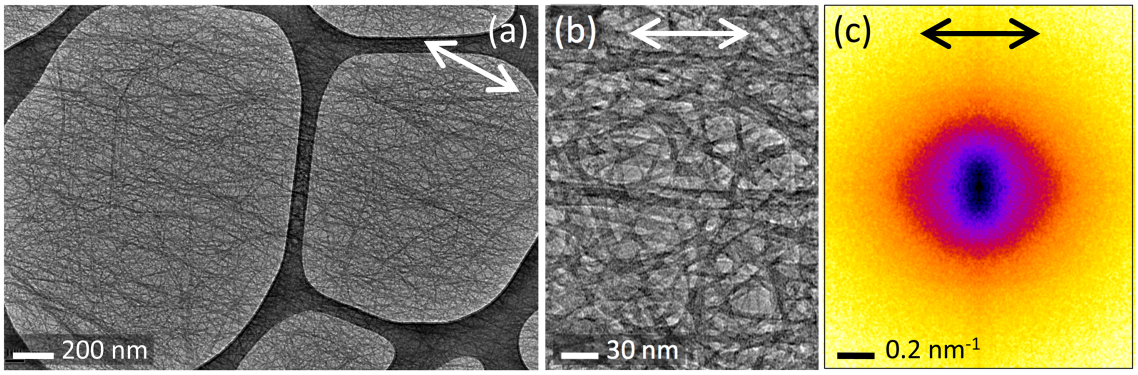

Figure S6 - (a) Coarse TEM image, (b) a higher resolution TEM image, and (c) the digital structure factor based on TEM. For each image, the flow/alignment direction is indicated by the arrow.

Characterizing SWCNT Alignment through TEM and Raman

As noted above, the alignment of the SWCNTs in response to shear was queried using polarization dependent UV-Vis absorption (Fig. S2). In addition, we used TEM (Fig. S6), and polarization-dependent Raman scattering near the G-band (Fig. 6c, main text). Typical TEM images of a sheared film are shown in Fig. S6. The digital structure

factor (Fig. S6c, defined as $|F|^2$ where F is the FFT of the TEM image computed in ImageJ) shows how the degree and direction of alignment vary with length scale, where the anisotropy becomes inverted in reciprocal space. To quantify SWCNT alignment, Raman spectroscopy was performed on a Renishaw inVia microscope using a 633 nm laser with a 20 μm diameter spot size. The incident and scattered polarization were varied to measure the intensity of the dominant G-band peak in three different scattering configurations, *VV*, *HH*, and *VH*. The order parameter, *S*, can be extracted from the polarization-dependent Raman G-band intensity using

$$S = \frac{I_{VV} - I_{HH}}{I_{VV} + I_{HH} + 2I_{VH}} \qquad \text{(S1)}$$

under the assumption of simple 2D (in-plane) orientation, or

$$S = \frac{3I_{VV} + 3I_{VH} - 4I_{HH}}{3I_{VV} + 8I_{HH} + 12I_{VH}} \qquad \text{(S2)}$$

under the assumption of 3D uniaxial alignment, where I_{XY} denotes the G-band Raman intensity measured with the incident polarization along *X* and the analyzing polarization along *Y* [*X*, *Y* = *V* ('vertical' or parallel to alignment), *H* ('horizontal' or perpendicular to alignment)].[8] For the film associated with the data in Fig. 6c of the main text, we obtain *S* = 0.53 from Eq. (S1) and *S* = 0.42 from Eq. (S2), where these values were typical of the films used in this study.

References

1. C. Y. Khripin, J. A. Fagan, M. Zheng, Spontaneous Partition of Carbon Nanotubes in Polymer-Modified Aqueous Phases. *J. Am. Chem. Soc.* **135**, 6822-6825 (2013).

2. J. A. Fagan, C, Y. Khripin, C. A. Silvera Batista, J. R. Simpson, E. H. Hároz, A. R. Hight Walker, M. Zheng, M. Isolation of Specific Small-Diameter Single-Wall Carbon Nanotube Species via Aqueous Two-Phase Extraction. *Adv. Mater.* **26**, 2800-2804 (2014).

3. J. M. Harris, M. R. Semler, S. May, J. A. Fagan, E. K. Hobbie, Nature of Record Efficiency Fluid-Processed Nanotube–Silicon Heterojunctions. *The Journal of Physical Chemistry C* **119**, 10295-10303 (2015).

4. V. A. Davis, A. N. G. Parra-Vasquez, M. J. Green, P. K. Rai, N. Behabtu, V. Prieto, R. D. Booker, J. Schmidt, E. Kesselman, W. Zhou, et al. True Solutions of Single-Walled Carbon Nanotubes for Assembly into Macroscopic Materials. *Nat. Nanotechnol*. **4**, 830-834 (2009).

5. A. N. G. Parra-Vasquez, N. Behabtu, M. J. Green, C. L. Pint, C. C. Young, J. Schmidt, E. Kesselman, A. Goyal, P. M. Ajayan, Y. Cohen, et al. Spontaneous Dissolution of Ultralong Single- and Multiwalled Carbon Nanotubes. *ACS Nano* **4**, 3969–3978 (2010).

6. D. S. Hecht, A. M. Heintz, R. Lee, L. Hu, B. Moore, C. Cucksey, S. Risser, High Conductivity Transparent Carbon Nanotube Films Deposited from Superacid. *Nanotechnology* **22**, 075201 (2011).

7. X. Li, Y. Jung, K. Sakimoto, T. Goh, M. A. Reed, A. D. Taylor, Improved Efficiency of Smooth and Aligned Single Walled Carbon Nanotube/Silicon Hybrid Solar Cells. *Energy Environ. Sci.* **6**, 879 (2013).

8. C. Zamora-Ledezma, C. Blanc, M. Maugey, C. Zakri, P. Poulin, E. Anglaret, Anisotropic Thin Films of Single-Wall Carbon Nanotubes from Aligned Lyotropic Nematic Suspensions. *Nano Lett.* **8**, 4103 (2008).